Jan Dutkiewicz, Wojciech Maziarz
Institute of Metallurgy and Materials Science
Polish Academy of Sciences, Kraków

MECHANICAL ALLOYING AND CONSOLIDATION OF NANOCRYSTALLINE TiAl AND NiAl BASE INTERMETALLICS

Key words

mechanical alloying , hot pressing, electron microscopy, TiAl, NiAl base alloys

Abstract

TiAl intermetallics containing additions of V, Cr and Nb and NiAl containing Ti, Fe additions were obtained from elementary powders by ball milling in a high energy planetary mill. In TiAl base alloys amorphous structure developed after 40 hours of milling and V and Nb additions accelerated this process, while Cr retards and forms bcc inclusions. NiAl alloys formed after milling nanocrystalline NiAl phase of B2 structure. Consolidation was performed using hot pressing or pulsed plasma sintering. The latter method allowed to obtain well developed nanocrystalline structure of average size 50 nm of TiAl and Ti_3Al phases.

Streszczenie

Związki międzymetaliczne na osnowie TiAl z dodatkami V, Cr i Nb oraz NiAl z dodatkami Fe i Ti uzyskiwano przez mielenie w wysoko-energetycznym młynie kulowym startując z proszków czystych metali. W stopach TiAl uzyskano po 40 godzinach mielenia strukturę amorficzną , a dodatki V, Nb przyspieszają ten proces, podczas gdy Cr opóźnia tworząc nanokrystaliczne wydzielenia o strukturze A2. Stopy o składzie NiAl tworzą po mieleniu nanokrystaliczne proszki o strukturze B2 NiAl. Konsolidację proszków prowadzono stosując prasowanie na gorąco, lub pulsowe spiekanie plazmowe. Ta ostatnia metoda doprowadziła do struktury nanokrystalicznej o średniej wielkości 50 nm ziaren TiAl i Ti_3Al.

1. Introduction

Intermetallic alloys based on γ-TiAl are of interest as light weight, high temperature materials, because of their low density, high melting temperature, good high temperature properties and oxidation resistance. These features in combination with their low density allow higher working temperatures, lead to improved operation efficiency and fuel saving in advanced transportation systems [1-4]. Unfortunately they are brittle at temperatures lower than 700°C [5,6]. The alloys are therefore difficult to fabricate by conventional ingot metallurgy and therefore powder metallurgy offers potential of minimizing processing problems and cost [1]. The Mechanical Alloying (MA) is an important technique for preparation of titanium aluminides powders [2,7]. The milling of

powders of composition close to γ-TiAl leads to the amorphous phase [2,7-8] or a hexagonal supersaturated solid solution [9]. The addition of Nb and Mn to γ-TiAl intensifies the process of amorphization [8-12] what allows to shorten

the time. The alloying additions modify mechanical properties of γ-TiAl intermetallics [2,3,11]; such as Mn, Cr, Nb are increasing yield strength while boron and vanadium fracture toughness [14]. The consolidation of TiAl base powders performed by hot pressing [15-17] leads to dense $\alpha_2 + \gamma$ type intermetallics with less than 1% porosity when Hot Isostatic Pressing (HIP) is applied. The higher the pressure and lower the temperature the finer grain size can be obtained [18].

In the nickel aluminium alloy system, equiatomic NiAl (B2-phase) of high melting temperature and low density (5.9 g/cm^3) and low affinity to carbon is considered for potential applications for gas turbine engines or coal burner elements [18]. Mechanical alloying (MA) permits to obtain amorphous or nanocrystalline phases in Ni-Al [19] systems. The homogenous fine powder particles after milling are considered as superior material for consolidation, since they usually result in a nanocrystalline structure with better plasticity than conventionally cast alloys [18-20]. In the case of milled NiAl base powder subsequent consolidation has been accomplished by means of hot pressing [21,22] or shock wave compaction [18,22]. The application of a shock wave produces a high pressure of microsecond duration allowing to obtain bonding between powders resulting in compacted samples with a high density. Since the early 1990's alloys based on the Nb_3Al intermetallic

compound have been considered as potential materials for high temperature structural applications [23]. These materials show promise of performance beyond the current generation of nickel base super-alloys because of the compound's high melting point (2060°C) and moderate density (7.26 g/cm^3). In the binary Nb-Al system, the Nb_3Al compound is adjacent to the Nb-Al solid solution allowing us to address its very poor ductility and fracture toughness (below the ductile-to-brittle transition temperature, which is about 1000°C [24,25]), by processing ductile phase-toughened near Nb_3Al alloys [26]. Also, the Nb_3Al phase has broad potential for alloying providing an opportunity for significant improvements of mechanical properties of Nb_3Al-based alloys [27].

In the present paper structure changes during ball milling of several TiAl, NbAl and and NiAl base intermetallic alloys will be described and the effects of following various consolidation methods will be compared taking into account resulting structure, density and mechanical properties.

Ternary Ti-Al-X phase diagrams

Fig.1 shows the isothermal section at 1000°C of the ternary TiAlV phase diagram after [28] with marked alloys compositions studied in [17]. One can see that relatively large γ-TiAl range can be observed at this temperature. It affects ordering and phase composition of the $\gamma - TiAl$. Fig. 2 shows isothermal section of the ternary TiAlNb system at 1100°C. It shows a limited up to 20 at.% solubility of Nb in the γ-TiAl phase,

therefore it is interesting how it affects properties of this phase and development of structure during ball milling. Fig. 3 shows an isothermal section of the TiAlCr ternary phase diagram at 800°C with marked compositions studied in [33]. One can see that it is different from the two previous ones and the addition of chromium causes limitation of the range of the γ–TiAl phase and above 5 at.% of chromium mixture of several phases exists.

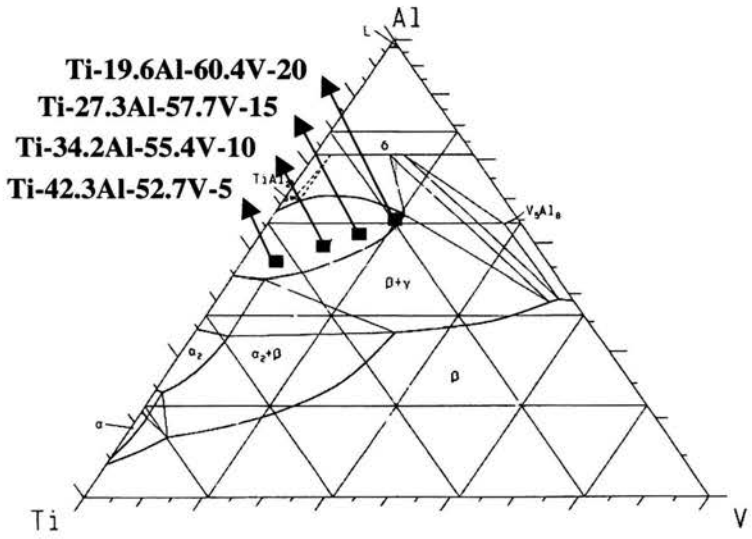

Fig. 1. Isothermal section at 1000°C of the ternary TiAlV system after [28]

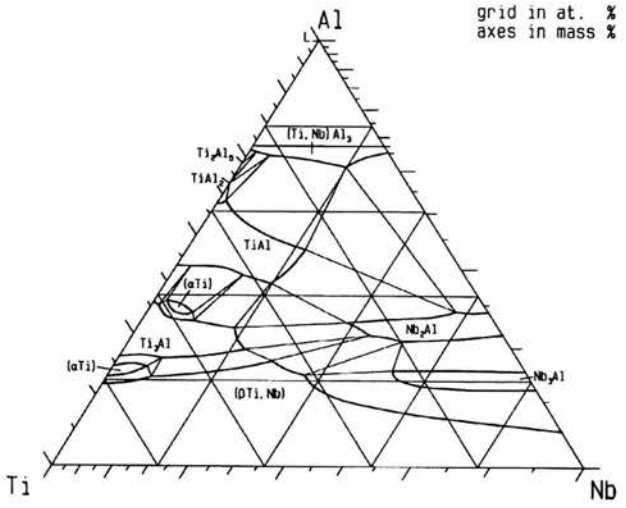

Fig. 2. Isothermal section at 1100°C of the ternary TiAlNb system after [28]

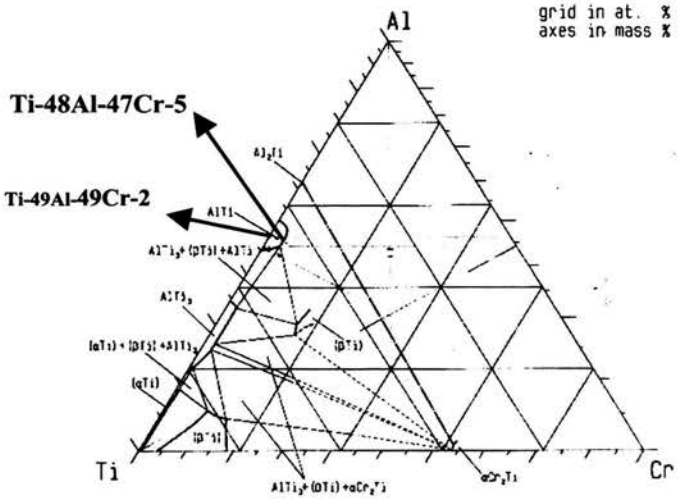

Fig. 3. Isothermal section of the TiAlCr ternary phase diagram at 800°C after [28]

Ternary Ni-Al-X phase diagrams

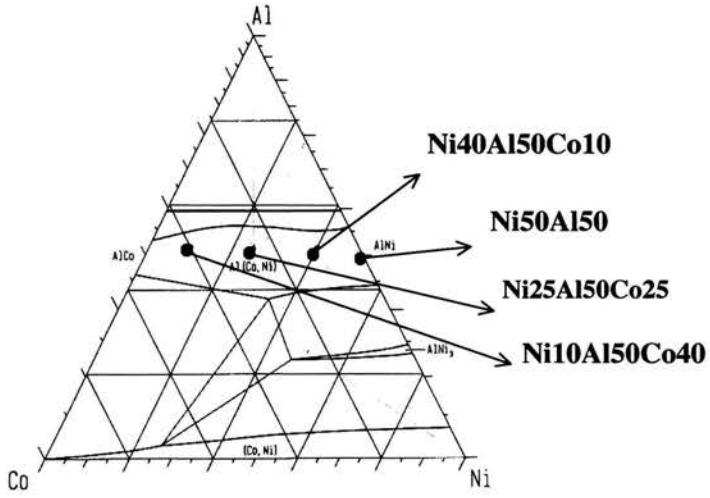

Fig. 4. Isothermal section of the NiAlCo phase diagram at RT after [28]

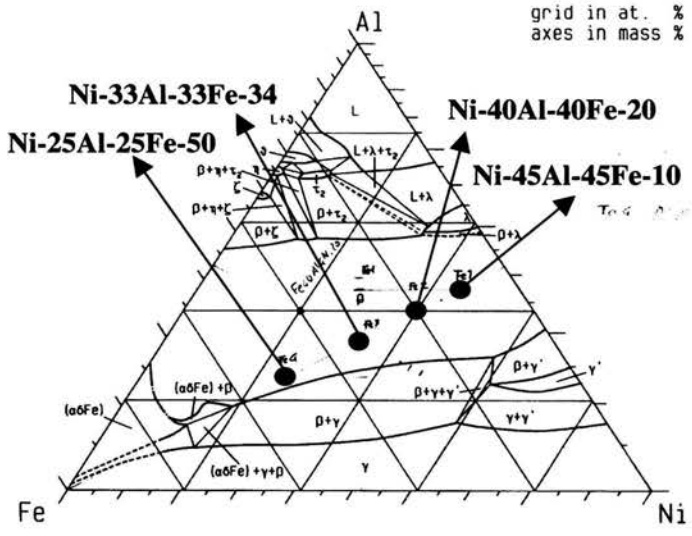

Fig. 5. Isothermal section of the NiAlFe ternary phase diagram at 1050°C after [28]

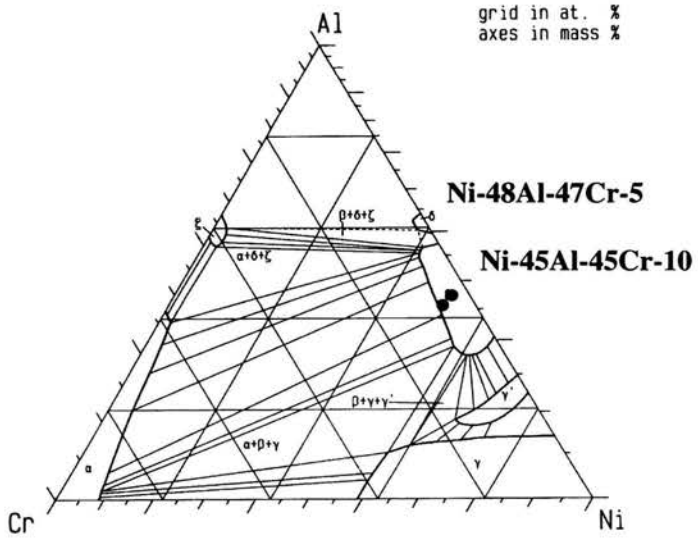

Fig. 6. Isothermal section of the NiAlCr ternary phase diagram at 1025°C after [28]

Figs 4-6 show ternary NiAl-X phase diagrams where X = Co, Fe and Cr with marked compositions studied in [36-38] respectively. One can see that addition of Co or Fe do not changes structure of NiAl and those systems form wide range of solid solutions NiAl-CoAl and NiAl-FeAl. Different situation is with the addition of chromium which addition larger than 10 at.% causes already formation of other phases what is expected not to improve mechanical properties, particularly ductility.

Mechanical alloying of TiAl

Fig. 7 shows a scheme of processes taking place during the ball milling process. During multiple hitting of powders particles first welding, then solid solutionizing and then fracturing of particles takes place. Optical micrographs in Fig. 8 shows various shapes and sizes (from a few μm until a few hundreds of μm) of elemental powders coming from various manufacturing processes of powders. Already after 5 hours of ball milling in the high energy planetary mill the corresponding micrographs show that they become much larger approaching size of 1 mm due to welding process of various powders particles. In the next stages phase transitions and solutionizing processes takes place within powders particles due to multiple deformation processes what finally lead to their hardening and fracturing. It can be seen in the Fig. 9 that in alloys containing 5 –20 at.% of vanadium that changes of particles size are similar in all alloys.

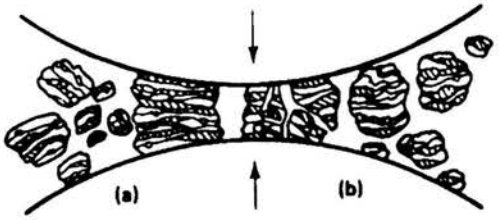

Fig. 7. Scheme of structure changes during ball milling of elemental powders

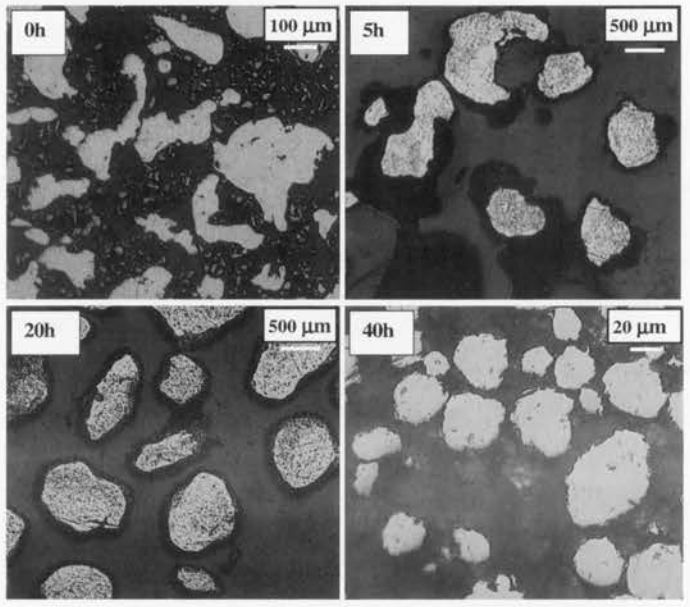

Fig. 8. Optical microstructures of powder particles of the alloy TiAlV5 (as marked in Fig.1) after indicated milling time in the planetary mill

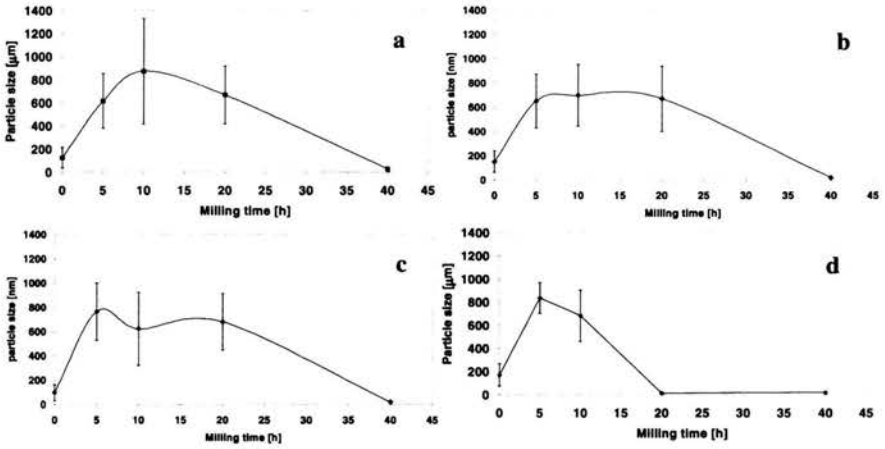

Fig. 9. Relationship of the powders particles versus milling time for alloys V5(a),V10(b),V15(c) and V20(d)

The particles grow up to about 5 hours of milling, then size stabilize and after 10-20 hours of milling the size of particles decreases down to 20 nm. As presented in Fig.10 the increase of hardness takes place in two stages. The first one is connected with the initial growth of particles and solid solution formation; then formation of plateau is connected with a stabilization of particle size. The hardness stabilisation was observed at the level of $HV_{0.02}$ = 400 for V5 and V10 and at $HV_{0.02}$ = 500 for V15 respectively. The second stage of particle growth occurs after 20 hours of milling and is connected with phase transitions and crystal refinement. The maximum hardness of the V5, V10, V15 and V20 aftter 40 hours of milling were $HV_{0.02}$ = 826, 716, 955 and 871 respectively. As compared with the results of R. A. Varin, obtained for AlMnTi system [29], an increase of micro-hardness of both the outer layer in powder particles with a core and the "no core" particles was noted.

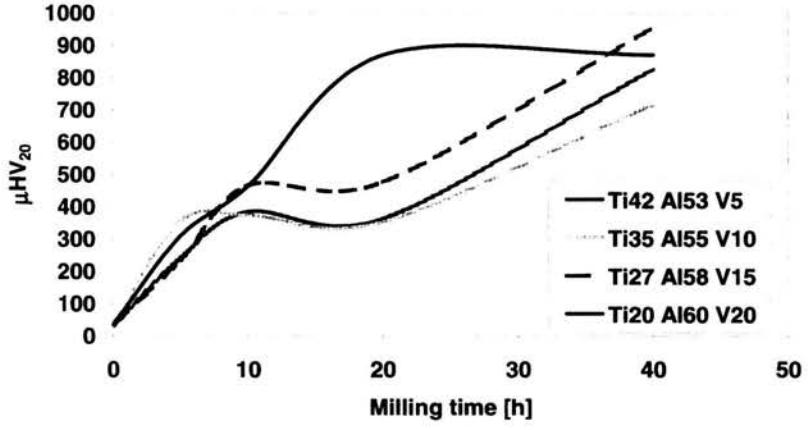

Fig. 10. Hardness versus milling time for alloys TiAl5V, TiAl10V, TiAl15V and TiAl20V

This microhardness increase is mostly due to work-hardening of the particles (Fig. 8) and in the final stages due to amorphization process which lead to very high hardness as in the bulk amorphous alloys [29].

In order to follow the structure changes during milling X-ray diffraction studies allow to identify structure changes (Figs. 11, 12). In the early stage of milling up to 5 hours the broadening of all peaks and decreasing their intensity was observed. It suggests that milling results in increasing of lattice strain and decreasing crystallite size what is characteristic for the early stages of the mechanical alloying process. Further milling up to 10 hours caused a disappearance of titanium and vanadium peaks and shifting of aluminium peaks toward lower values of 2Θ angles. In the case of alloys with up to 15 at.% vanadium only a decrease of crystallite size of Al(Ti, V) solid solution was observed after 20 hours of milling. However, in the case of alloy with 20 at. % of vanadium the formation of some metastable phase was detected, characterised by one broad peak with two maxima in the range between 43 and 54°. After 40 hours of milling in all alloys an almost fully amorphous phase was observed. However in the alloy of highest vanadium content no crystallite peaks can be seen after longest milling time.

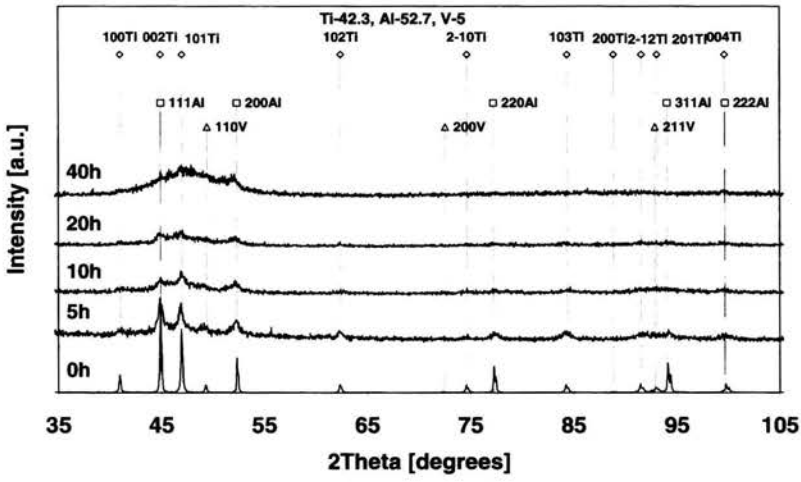

Fig. 11. Set of X-ray diffraction pattern of Ti-42.3, Al-52.7, V-5 after different milling time

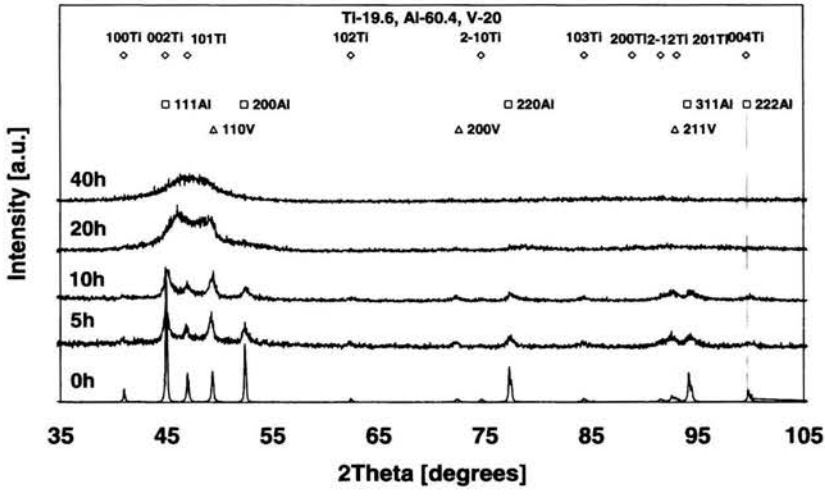

Fig. 12. Set of X-ray diffraction pattern of TiAlV20 after different milling times

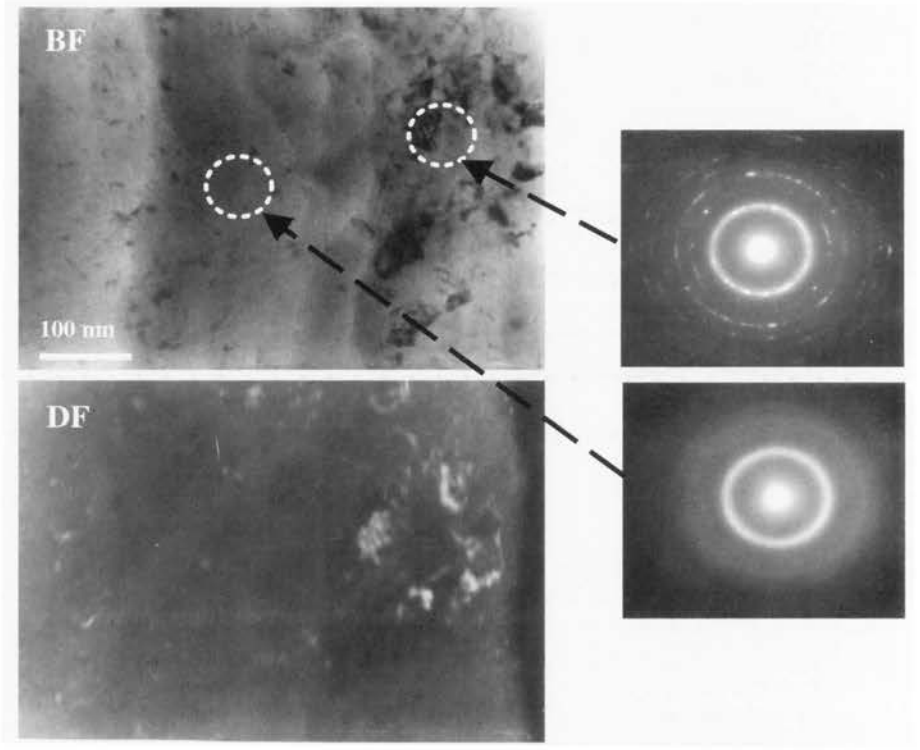

Fig. 13. Bright and dark field transmission electron micrographs and corresponding SADP from 40 hours ball milled TiAl15V alloy

Fig.13 shows a set of bright and dark field transmission electron micrographs and corresponding selected area diffraction patterns (SADP) from 40 hours ball milled TiAl15V alloy. One can see a nonhomogeneity of the sample. Diffraction pattern from the homogeneous central area of the sample shows typical diffused ring as from amorphous structure, while that from the right side showing dark particles shows rings according to interplanar distances: d_1=0.215 nm, d_2= 0.147 nm, d_3=12 nm, which corresponds to the β-V(Ti, Al) solid solution of the lattice parameter a= 0.303 nm. Another characteristic feature of ball milled

samples are stripes running in Fig.13 from the top to the bottom. They result from multiple deformation during milling leading finally to almost homogeneous structure, however showing this type of contrast most probably due to fine chemical composition changes.

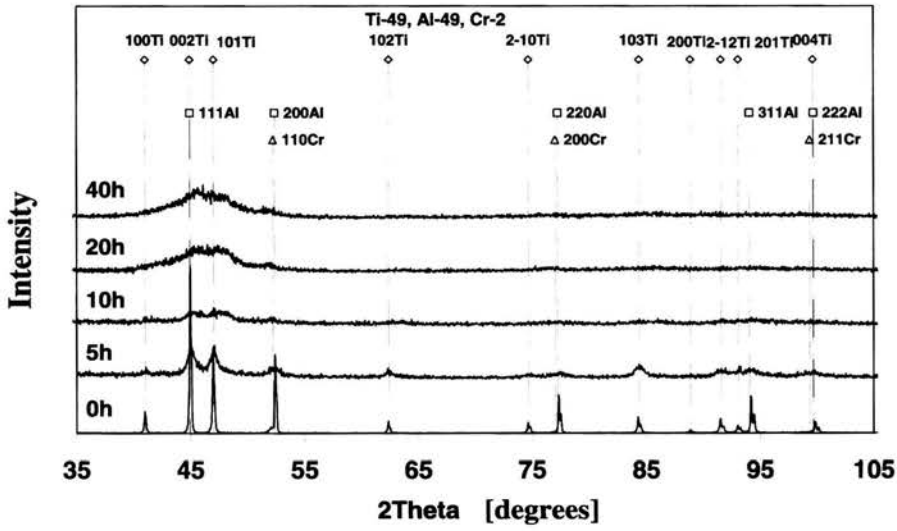

Fig. 14. Set of X-ray diffraction pattern of alloy Ti-49Al-49Cr-2 after different milling times

Contrary to the effect of niobium [11], the higher the chromium addition, the stronger are reflections from crystalline phases in spite of that the alloys are from the solid solution range similarly like in the case of other additions. This indicate that various elements have a different influence on the amorphization behaviour of TiAl alloys.

Figs.14 and 15 show a set of X-ray diffraction pattern of the alloy Ti-49Al-49Cr-2 and Ti-48Al-47Cr-5 after different milling times. One can see that contrary to the addition of vanadium or niobium [11] increasing

of the addition of chromium causes increase of the intensity of peaks from crystalline phases. This indicate that the addition of chromium retards the amorphization process during ball milling.

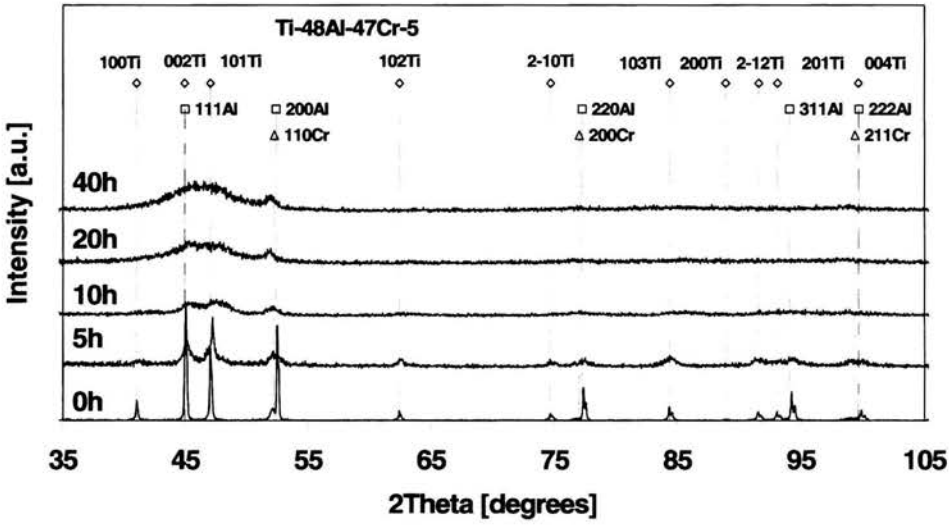

Fig. 15. Set of X-ray diffraction pattern of Ti-48Al-47Cr-5 after different milling times

In order to identify the structure of milled powders very interesting results bring high resolution transmission electron microscopy as presented in Fig. 16 It shows a micrograph from the alloy Ti-49Al-49Cr-2 after 40 hours of milling. It shows about 50 nm large crystal marked by a white dotted line surrounded by the amorphous matrix. Within the amorphous phase one can identify short range ordering (marked by a white circle) of size of a few nanometers. The Fourier transform shown in the corner shows that spots are under the angle of 60°. The distance of fringes corresponds to the 110 plane of chromium therefore the crystal

can be identified as chromium or chromium rich crystal. The chemical microanalysis confirms enrichment of nanocrystals in chromium.

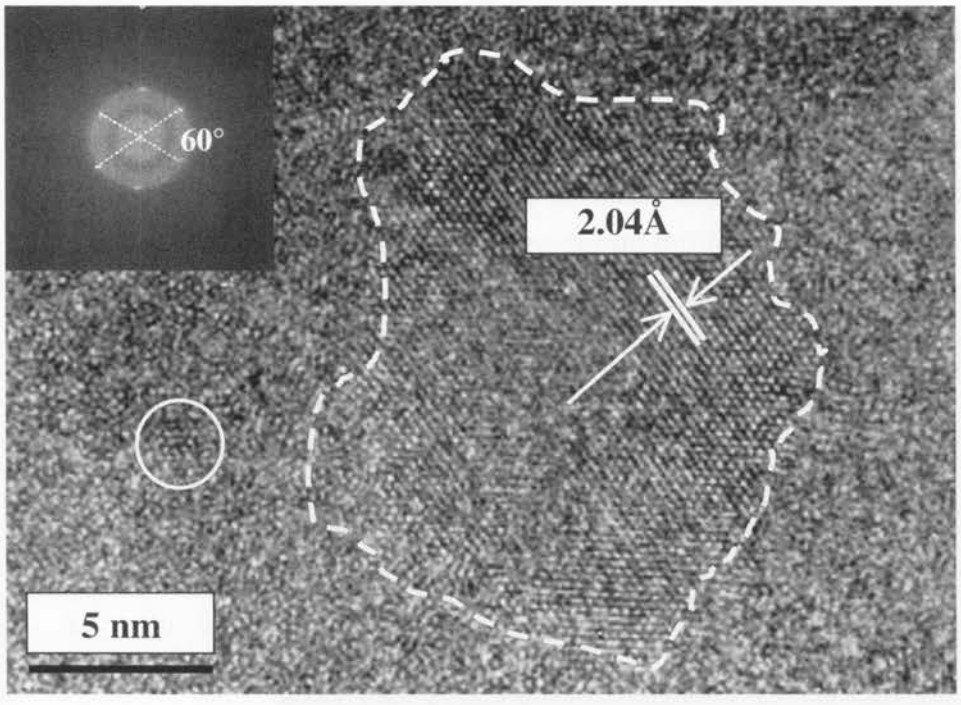

Fig. 16. High resolution transmission electron micrograph of the alloy Ti-49Al-49Cr-2 after 40 hours of milling

Fig. 17 shows high resolution micrograph and corresponding Fourier transform of Ti-48Al-47Cr-5 alloy after 40 hours of milling showing lamellar $\alpha_2/\gamma/\alpha_2$ region embedded in amorphous matrix. The phases were identified by measurements of the interplanar distances of α_2 and γ phases and indexing of diffraction pattern resulting from the Fourier transform analogical like in [30] where $<111>\gamma \parallel <11\text{-}20>\alpha_2$. Presence

of crystals in mechanically alloyed TiAlCr alloy after mechanical alloying was also observed by Ovecoglu et al [31], however no phases were identified due to very fine dimensions of crystals. At the right upper and lower corners the contrast suggests presence of amorphous phase. Synthesis of either TiAl or Ti_3Al phases was not observed so far and it can be explained only by nucleation of these phases at Cr crystals which do not mix with solute elements during milling.

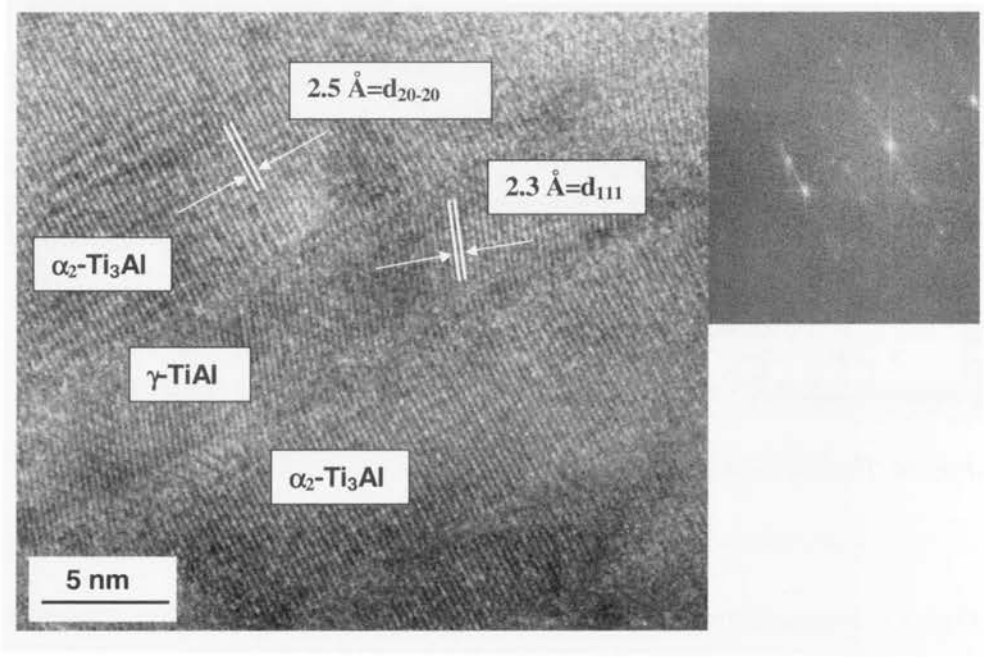

Fig. 17. HREM micrograph and corresponding Fourier transform of Ti-48Al-47Cr-5 alloy after 40 hours of milling shows lamellar $\alpha_2/\gamma/\alpha_2$ region embedded in amorphous matrix

Mechanical alloying of NiAl-X alloys

Fig. 18 shows a set of optical micrographs of Ni25Al50Co25 alloy after different milling times. One can see that already after 2 hours elemental powders weld together forming large particles similarly like in the case of TiAl-X alloys. The elemental constituents become much finer after 20 hours of milling without significant changes of the size of the particle. After 40 hours one cannot distinguish structure constituents and at the same time particles start to fracture during milling leading to their refinement.

The X-Ray Diffraction XRD patterns after 80 h of milling (Fig. 19) allow to identify one phase, i.e. Al(Ni, Co) intermetallic B2 solid solution structure. However, optical microscopy observations show that there are still regions inside powders visible where a contrast from almost pure elements is present. Therefore, the milling was continued up to 160 h. After this time no significant changes of diffraction curves were observed, indicating that the nanocrystalline Al(Ni, Co) solid solution is highly stable and can probably not be amorphized through further milling. The intensities and the shape of the peaks of Al(Ni, Co) after 160 h of milling are not changed for all investigated alloys. This indicates that the alloys in this region of the ternary phase diagram can be produced for a wide range of compositions as nano-sized intermetallic compounds.

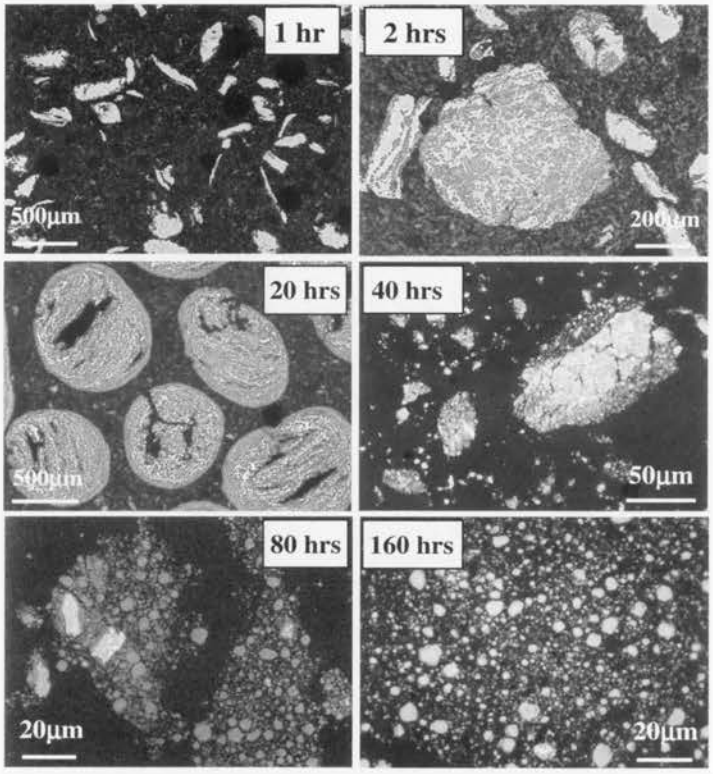

Fig. 18. Optical micrographs showing powder morphology of alloy Ni25Al50Co25 after different milling times

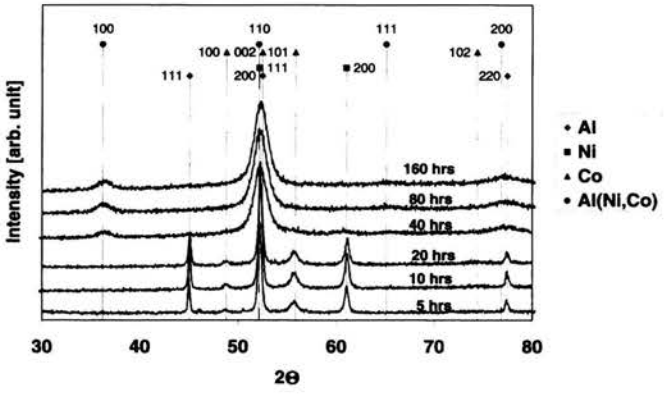

Fig. 19. XRD patterns of Ni25Al50Co25 alloy after different milling times

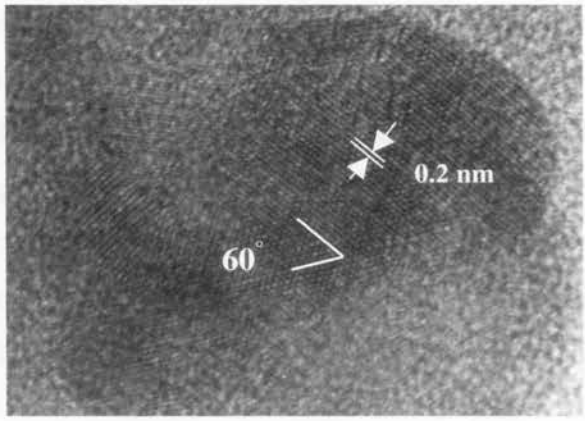

Fig. 20. HREM micrograph of the microstructure of alloy Ni40Al50Co10 after 160 h of milling

Fig. 20 shows a high resolution TEM micrograph of the sample Ni40Al50Co10 milled for 160 hours. From the distance of the lattice fringes, which is equal to about 0.2 nm, and from the angle of fringe crossing, which is equal to 60°, one can identify the crystals as Al(Ni, Co) intermetallics solid solution with B2 structure. The size of the crystals varies in different regions and can be between 2 and 7 nm, being in a good agreement with the X-ray data.

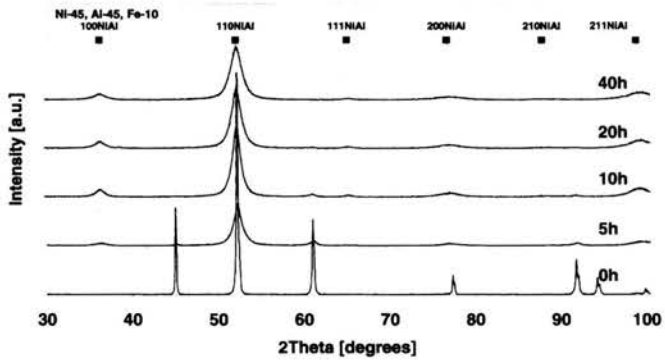

Fig. 21. Set of X-Ray diffraction pattern from powders of composition Ni45Al45Fe10 after different milling times

Fig. 21 shows a set of X-Ray diffraction pattern from elemental powders of composition Ni45Al45Fe10 after different milling times. One can see that already after 5 hours of milling synthesis of (Ni,Co)Al solid solution is observed. Further milling causes only broadening of peaks. A clear presence of superpattice 100 spot should be noted contrary to the X-ray diffraction pattern from Ni25Al25Fe50 where no ordered reflections can be seen. It is contrary to the expectations based on the phase diagram [28], where no differences in the ordered solid solution structure were marked in a wide range of compositions.

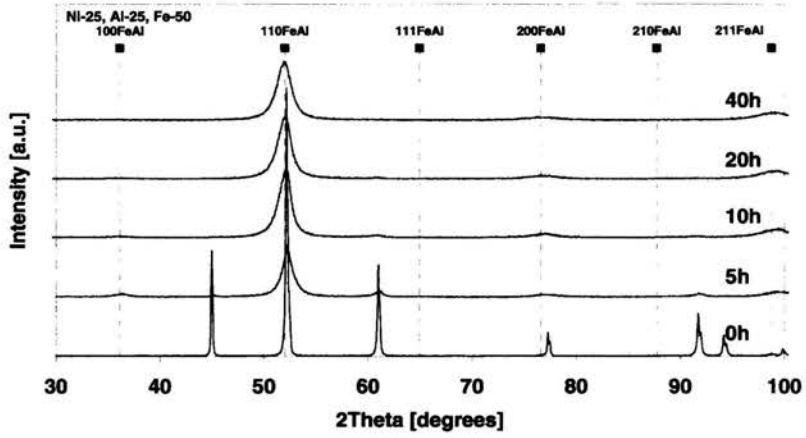

Fig. 22. Set of X-Ray diffraction pattern from powders of composition Ni25Al25Fe50 after different milling times

Fig. 23 shows TEM microstructures from Ni40Al40Fe20 alloy powder milled for 40 hours showing nanosize crystals of NiAl phase. One can clearly see ring corresponding to 100 superlattice reflections confirming X-ray diffraction data concerning ordering of (Ni,Fe)Al phase. The size of crystals can be estimated between 5-10 nm. The high resolution

micrograph taken from the powder particle of Ni45Al45Fe10 ball milled alloy (Fig. 24) show several fringes running in various directions. Fourier transform from HRTEM image shows rings corresponding to d_{001} and d_{011} lattice spacings confirming results of SADP and X-ray diffraction concerning ordering of (Ni,Fe)Al phase. Additionally some moire pattern can also be seen due to overlapping of crystals. TEM studies of alloys containing 34-50 at.% Fe do not show ordered reflections.

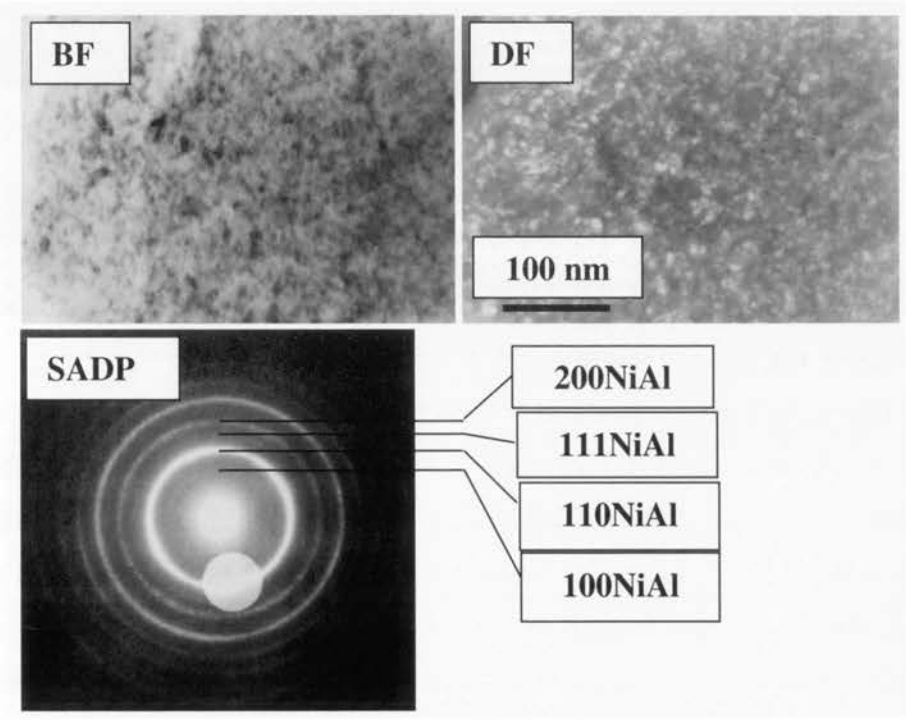

Fig. 23. Bright field, dark field and electron diffraction pattern from Ni40Al40Fe20 alloy powder milled for 40 hours showing nanosize crystals of NiAl phase

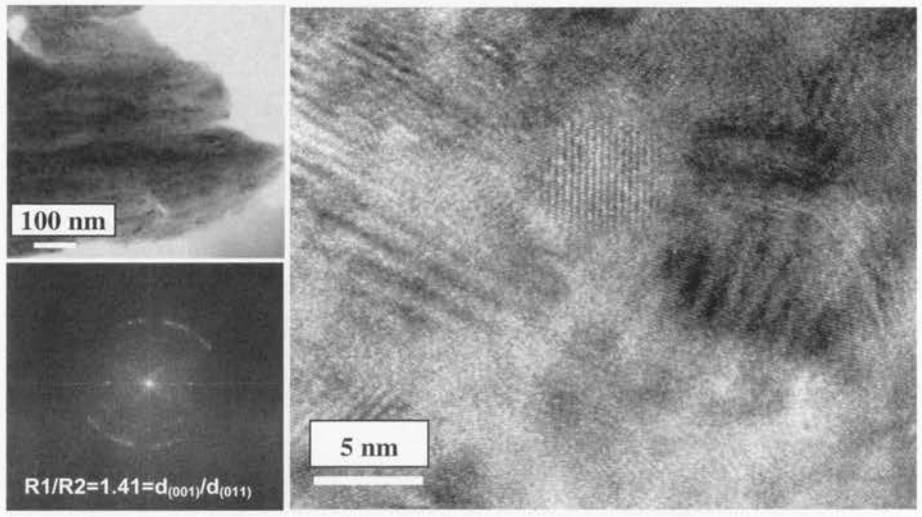

Fig. 24. Bright Field and HRTEM micrographs of powder particle of Ni45Al45Fe10 ball milled alloy. Fourier transform from HRTEM image shows rings corresponding to d_{001} and d_{011} lattice spacings

Consolidation of mechanically alloyed nanocrystalline powders using hot pressing

TiAl48% ball milled powders with 15 nm grains were consolidated to 99.5% of the theoretical density at 800°C under 200 MPa using Hot Isostatic Pressing (HIP) technique [27]. The grain size increase up to 150 nm was observed. In [33] uni-axial hot pressing at 700°C was applied to consolidate the nanocrystalline milled powders were under 200MPa in argon flow atmosphere. The optical microstructures in binary convolutions (Fig. 25) were used for separation of pores in compacts and calculation the area fraction of bulk phases. One can see that the pores are inhomogeneously distributed and two sizes of pores can be distinguished i.e. small amount of big ones in size ranged from

20 to 50 μm and network of very small pores below 1 μm, usually located on particle's. The character and distribution of pores influences densification of samples. It was shown that bulk phases occupy about of 94 % area fraction. Fig. 26 presents X-Ray diffraction pattern of Ti-52.7Al-5V sample uni-axially hot pressed at 700°C under 200 MPa. The two phase structure $\gamma+\alpha_2$ with higher fraction of γ was identified. Peaks are relatively broad indicating nanometer range structure in the sample.

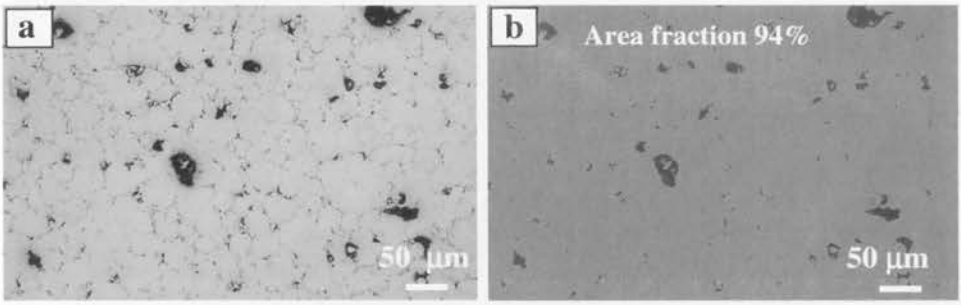

Fig. 25. (a) Optical microstructure of Ti-52.7Al-5V sample uni-axially hot pressed at 700°C under 200 MPa and (b) corresponding binary image

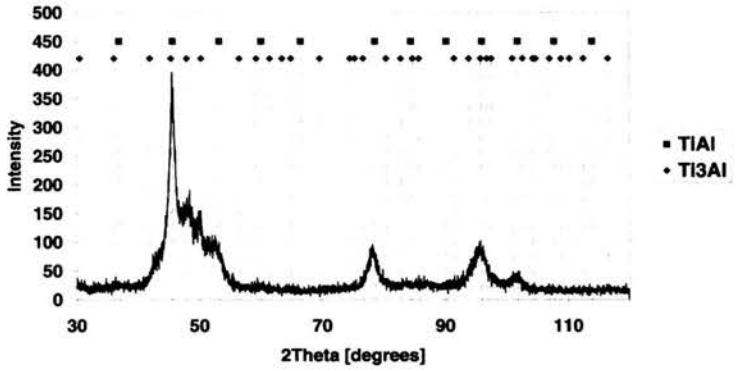

Fig. 26. X-Ray diffraction pattern of Ti-52.7Al-5V sample uni-axially hot pressed at 700°C under 200 MPa

Fig. 27 shows TEM micrographs which allowed to identify the nanometer range grain structure with a mean size of about 20-30 nm and with slightly elongated shape. The diffraction pattern has shown a ring like pattern without preferred grain orientation confirming presence of $\gamma+\alpha_2$ phases.

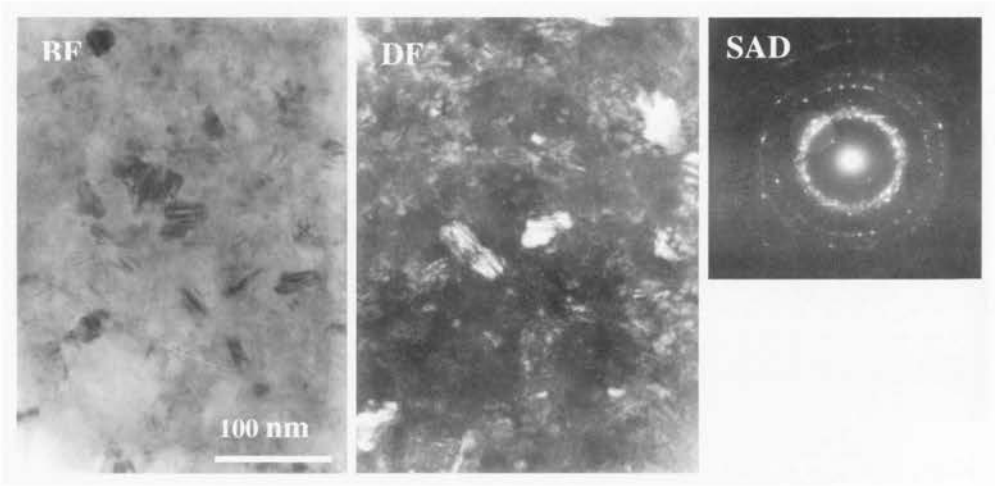

Fig. 27. Bright field (left) and dark field (right) TEM microstructures and corresponding Selected Area Diffraction Patterns (SADP) of Ti-52.7Al-5V alloy after hot pressing at 700°C under 200MPa

Similar electron microstructure shows Ti-48Al-47Cr-5 sample (Fig. 28) hot pressed under identical conditions as the previous one. It shows average grain size below 100 nm and it consists of γ and α_2 phases similarly as the previous one with vanadium as confirmed by X-ray studies. Unfortunately only slightly better density of 96% was attained, still far from that when using HIP.

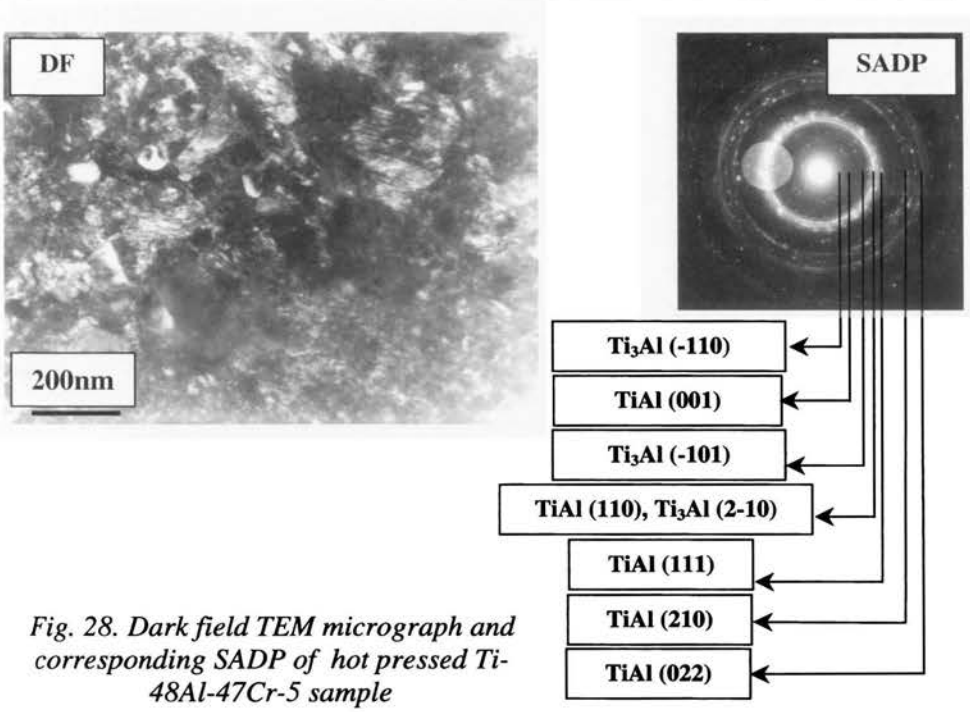

Fig. 28. Dark field TEM micrograph and corresponding SADP of hot pressed Ti-48Al-47Cr-5 sample

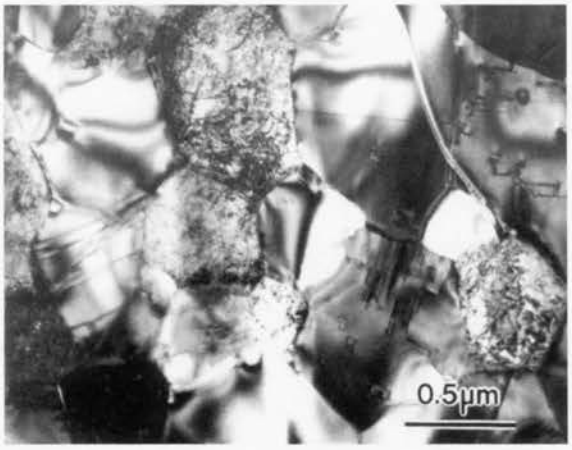

Fig.29.Transmission electron microstructure of the sample Nb18Al hot pressed at 1150°C

Fig. 29 shows transmission electron microstructure of the alloy Nb18Al hot pressed at 1150°C.

A mixture of Mb_2Al and Nb_3Al phases can be seen, the average grain size is close to 0.5 μm what is much more than observed in TiAl base alloys (Figs. 27, 28) hot pressed at lower temperatures. However, the ultimate compression strength and elongation at room temperature (Fig. 30) are similar that observed for above described TiAl alloys in spite of their smaller grain size what can be explained by their higher porosity.

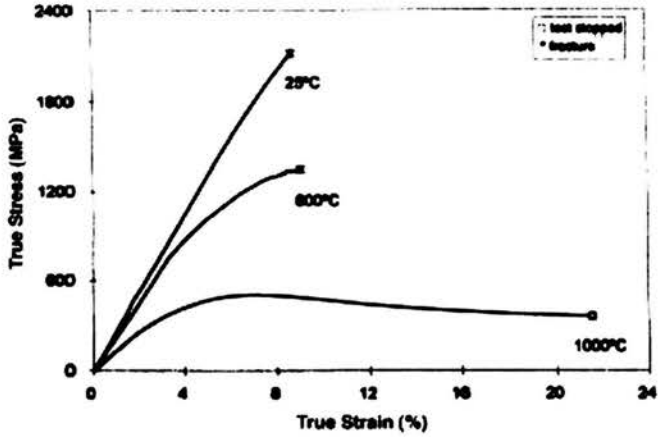

Fig. 30. Compression tests of Nb18Al alloy at various temperatures after [27]

Consolidation of mechanically alloyed nanocrystalline powders using pulsed plasma sintering

Fig. 31 shows a scheme of installation for pulsed plasma sintering at Department of Materials science Warsaw University of Technology. It allows heating of powder samples by electric current pulses under pressure of 60 MPa. The microstructure of the mechanically alloyed

samples of the TiAl alloy is shown in Fig. 31. The time of the impulse is 500 ms at the charging voltage of 8kV. The time of sintering is 3 min. Fig. 32 shows a two phase transmission electron microstructure of the γ-TiAl + α_2Ti_3Al of the Ti48Al alloy after pulsed plasma sintering. One can see that the grain size is similar like after hot pressing. The quantitative measurements based on several micrographs gave the average result 200 nm.

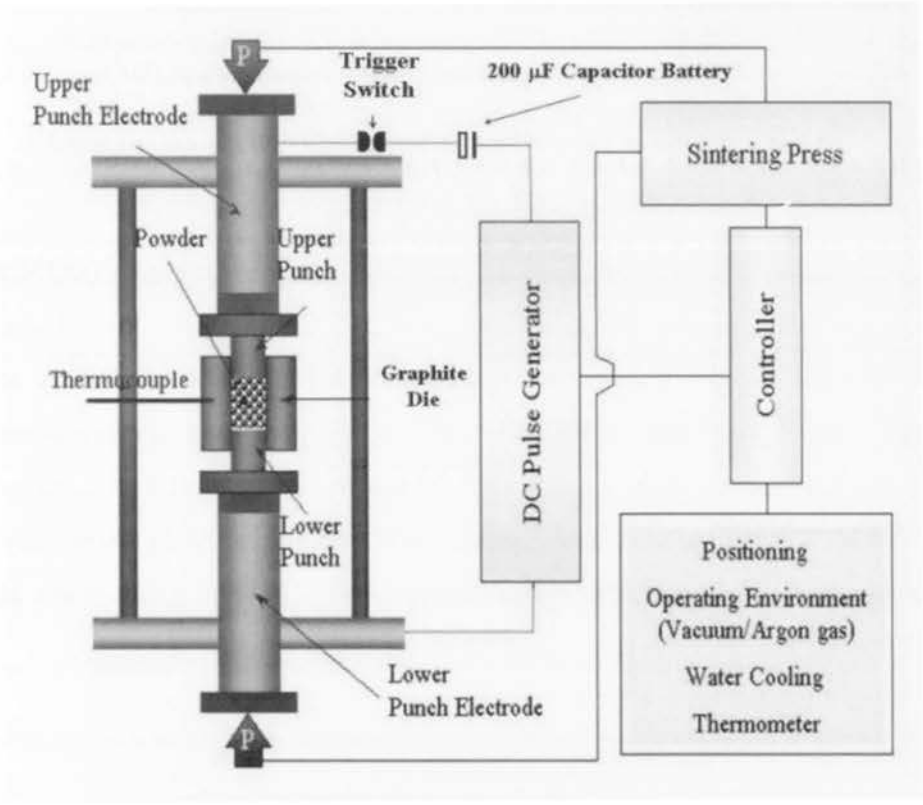

Fig. 31. Scheme of the apparatus for pulsed plasma sintering

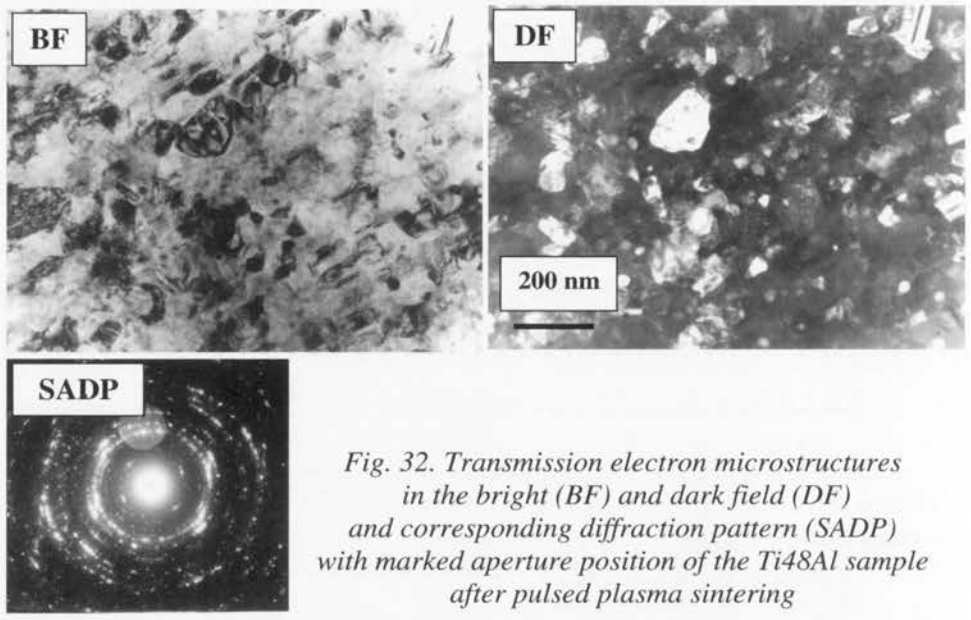

Fig. 32. Transmission electron microstructures in the bright (BF) and dark field (DF) and corresponding diffraction pattern (SADP) with marked aperture position of the Ti48Al sample after pulsed plasma sintering

Fig. 33 shows compression tests of the pulse plasma sintered TiAl5Cr alloy. One can see that alloys tested below 500°C show very low plastic deformation , below 1% but at higher temperatures it deforms easily at very low stress most probably due to superplastic deformation mechanism and grain boundary sliding mechanism. Similar behaviour was observed at TiAl and TiAlV plasma sintered alloys. Alloy show very high strength at room temperatures (above 1400 MPa) and much lower at 800°C.

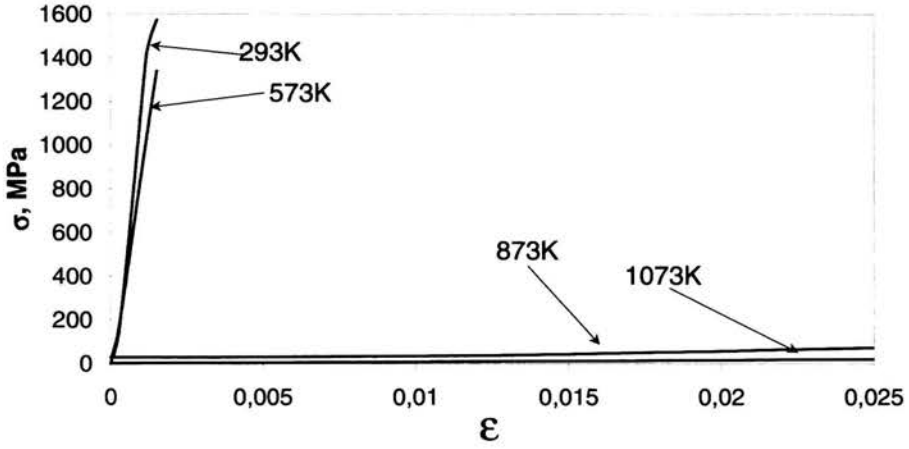

Fig. 33. Compression tests of pulse plasma sintered samples of TiAl5Cr alloy at various temperatures

Shock consolidation of mechanically alloyed nanocrystalline NiAl powders

T. Chen et all [34] shockwave compacted mechanically alloyed β-NiAl ordered phase with mean crystalline of 10nm. Shockwave compaction was accomplished using single stage gas gun. Impact experiments were performed using an aluminum projectile and a 5 mm thick stainless steel flyer plate accelerated in the 80 mm diameter gas gun, at an impact velocity measured to be approximately 400 m/s. Following an initial pressure wave of 1 GPa, a bulk peak pressure of 4-6 GPa was predicted due to two dimensional radial wave focusing effects. The samples were recovered in the form of 10 mm diameter by 3 mm thick discs. The shock consolidated NiAl powder compacts had both micro and macro cracks propagating radially outward from the compact axis. The densities of the shock compacted mechanically alloyed NiAl

powders were measured to be 4.81-4.88 g/cm^3, which is approximately 83% of the theoretical maximum density of B2-NiAl. The X-Ray diffraction experiments proved that the nanocrystalline NiAl phase of the mechanically alloyed powder was retained after shock compaction. The broadened diffraction patterns are attributed to the effects of the nanoscale crystallite size and retained residual stress. An SEM micrograph of a cross-section of the shock compacted sample, shown in Fig. 34 reveals the presence of voids, indicating that under the consolidation conditions used, complete densification is not achieved. The SEM micrograph of the fracture surface of the shock compacted sample, shown in Fig. 34(b), reveals that the fracture occurs along inter-particle boundary regions, leaving particles intact, confirming the lack of complete metallurgical bonding.

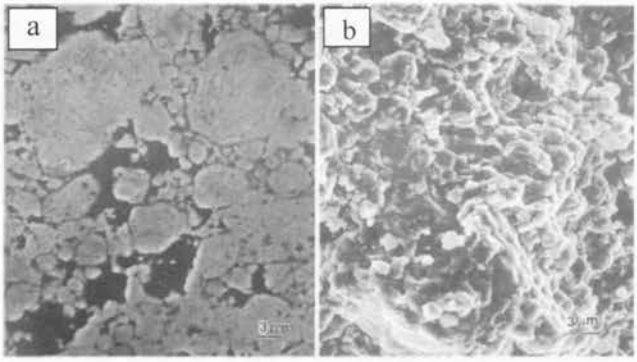

Fig. 34. SEM micrographs of shock-consolidated nanocrystalline NiAl: (a) cross-section, (b) fracture surface

The results of Vickers microhardness indicate that grain size refinement, from approximately 650 to 800 HV as average grain size changed from 27±18 nm (after 16 h ball milling) to 9±6 nm (after 48 h

ball milling). These measured microhardness values are much higher than that of coarse-grained polycrystalline NiAl (330 HV reported by Haubold et al. [35]).

Summary

Alloy NiAl10-20 ball milled for 40 hours develops nanocrystalline B2 ordered structure already after 5 hours of milling which becomes finer after longer milling. In the ball milled alloy NiAlFe30-50 disordered structure was detected using electron microscopy and confirmed using X-ray studies.

In TiAl base alloys formation of Al(Ti, X) solid solution was observed after 10 hours of milling in all alloys investigated. Longer milling amorphized most of material. Increase of third element content Like V or Nb caused faster and more complete amorphisation process during milling. The mean Vickers micro-hardness of powders after 40 hours of milling ranged from the $HV_{0.02}$ = 710 up to 955. The micro-hardness increases mostly due to work-hardening of the particles and in the final hours of milling due to amorphization process which lead to very high hardness as in bulk amorphous alloys.

The uni-axial hot pressing at of TiAl base alloys at 1000°C under 35 MPa of milled powders allowed to obtain compacts of 80 to 97% of the theoretical density and several μm grain size. The hardness of compacts increases with density reaching the maximum value of about HV_5=600. Similar microhardness was attained for NbAl alloys hot pressed at 1150°C. The structure of hot pressed material consists of spherical

α_2 grains separated by γ-TiAl containing vanadium. Uni-axial hot pressing at 700°C under 200 MPa of milled powders allowed to obtain a bulk samples with density of about of 94 % of theoretical one. The predominated two phase $\gamma+\alpha_2$ nanocrystalline structure was observed in hot pressed sample with the mean grain size of about 100 – 200 nm. Additionally some larger grains with size of about 300nm of α_2-Ti_3Al phase were also distinguished. The mean micro-hardness reached $HV_{0.02}$ = 1480 for TiAl alloys containing up to 20% vanadium.

Pulsed plasma sintered TiAl base alloys allowed to obtain the average grain size slightly lower that hot pressed at 700°C, but much higher density of 98%. It caused higher strength (between 1400-1600 MPa) and a few percent ductility at room temperature. The strength at higher temperatures was similar to hot pressed ones, usually below 200 MPa at 800°C.

The shock consolidated NiAl powder compacts had both micro and macro cracks propagating radially outward from the compact axis. The densities of the shock compacted mechanically alloyed NiAl powders were measured to be 4.81-4.88 g/cm^3, which is approximately 83% of the theoretical maximum density of B2-NiAl. The Vickers microhardness varies from approximately 650 to 800 HV as average grain size changed from about 20 nm to about 8 nm. These measured microhardness values are much higher than that of coarse-grained polycrystalline NiAl (330 HV).

Acknowledgements

The partial financing of this work by the Project Nr PBZ-KBN-041/T08/2001 is gratefully acknowledged.

References

1. H.A. Lippsitt: High-Temperature Ordered Intermetallics Alloys, Materials Research Society Symposium, C.C. Koch, C.T. Liu and N.S. Stoloff, eds., Materials Research Society, Princeton, NJ, 1984, vol. 39, pp.351-64
2. F.H. Froes, C. Suryanarayana, and D. Elizier: J. Mater. Sci., 1992, vol. 27, pp. 5111-40
3. Y.-W. Kim: J. Met., 1995, vol. 47 (7), pp. 39-41
4. D.W. Mckee and S.C. Huang: High-Temperature Ordered Intermetallics Alloys IV, Materials Research Society Symposium, L.A. Johnson, D.P. Pope and J.O. G. Stiegler, eds., Materials Research Society, Princeton, NJ, 1990, vol. 213, pp.939-43
5. Sauthoff, Z. Metallkde, 77(1986) 654
6. Y-W Kim, Acta metal., 40 (1992) 1127
7. C. Suryanaryana and F.H. Froes, Mater. Sci Eng., Vol. A179/A180 (1994), p. 108.
8. Oehring, T. Klassen, and R. Bormann, J. Mater Res. Vol.8, (1993), p. 2819.
9. J. Dutkiewicz, W. Maziarz, R. Scholz, Inż. Mater., Nr 4 (123), (2001), p. 299.
10. J. Dutkiewicz, W. Maziarz, Inżynieria Materiałowa, No1, 22, (2001) 32-36
11. J. Dutkiewicz, W. Maziarz, Metallurgy on the turn of 20th century , editor K. Świątkowski, published by Committee of Metallurgy and Materials Science, Kraków AKAPIT 2002 str.448-453
12. J. Dutkiewicz, S. Schlueter, W. Maziarz J. Metastable and Nanocryst. Mat., 20-21, (2004) 127
13. Walkowiak, T. Sell, H. Mehrer, Z. Metallkd. 85, (1994), p. 5.
14. M. Barinov, J. Mater. Sci Letters Vol. 18, (1999) p. 923.

15. Guangxin Wang and M. Dahms, JOM 45 (1993 53
16. J.B. Yang, K.W. Teoh, W.S. Hwang Mater. Sci Technol., 13 (1997) 695
17. J. Dutkiewicz, W. Maziarz, Solid State Phenom., 101-102 (2005)117
18. T. Chen, J.M. Hampikian and N.N. Thadhani, Acta mater., 47 (1999) 2567
19. Kambara M., Uenishi K., Kobayashi K. F., J. Mater. Sci. 35 (2000) 2897-2905.
20. Calderon H.A., Garibay-Febles V., Cabrera A., Cabanas-Moreno J. G. and Umemoto M., Mater. Sci. Forum, Vols. 360-362 (2001), 229-234
21. S.G. Pyo, N.J. Kim, P. Nash, Mater. Sci Eng., (1994) A181-182 1169
22. S.C. Glade and N.N. Thadhani, Metall. Trans. 26A (1995) 2565
23. Anton DL, Shah DM. Mat Sci Eng 1992;A153:402.
24. Anton DL, Shah DM. Mater Res Soc Symp 1991;213:733
25. Rong TS, Horspool DN, Aindow M. Intermetallics 2002;10:1. Nomura N, Yoshimi K, Hanada S. In: Nathal MV et al, editor. Structural Intermetallics. Warrandale, USA: TMS, 1997. p. 923.
26. Tappin DK, Smith LS, Horspool DN, Aindow M. Acta Mater 1997;45:4923.
27. Dymek S, Dollar M, Leonard K. Mat Sci Eng 1997;A239-240:507.
28. P. Villars, A. pronce and H. Okamoto, Handbook of Ternary Phase Diagrams, Ed. ASM 1995
29. R.A. Varin, D. Wexler, A. Calka, L. Zbroniec, Intermetallics, Vol. 6, 1998, p.547.
30. P.J. Maziasz and C.T.Liu Metal mater rans. 29A (1998) 105
31. M.L. Ovecoglu, O.N. Senkov, N. Sriskhumbowornchai, F.H. Froes, Met. And mater. Trans 30A (1999) 751
32. M. Oehring, F. Appel, Th. Pfullmann, R. Bormann, Appl. Phys. Lett., 66 (1995) 941
33. J. Dutkiewicz, W. Maziarz paper presented in EMRS 2004
34. T. Chen, J.M. Hampikian and N.N. Thadhani Acta mater., 47 (1999) 2567

35. T. Haubold, T. Bohn, R. Birringer and H. Gleiter, Mater. Sci Eng. A153 (1992) 679
36. W. Maziarz, J. Dutkiewicz, J. Eckert, P. Vermaut, R. Portier, Proc. Conference for Applied Crystallography, Krakow ed.H. Morawiec, D, Stróż World Scientific, p.237
37. J. Dutkiewicz, L. Lityńska and W. Proc. 13th European Microscopy Congress Vol.2 p165-166
38. J. Dutkiewicz, W. Maziarz Presented on Polish-Japanese Symposium in Niedzica 29.09-2.10.2004 accepted for print in Archives of Materials Sci,